Korean J. Chem. Eng., 35(2), 394-408 (2018)
DOI: 10.1007/s11814-017-0292-x

pISSN: 0256-1115
eISSN: 1975-7220

Steam reforming of α-methylnaphthalene as a model compound of biomass tar over Ni-based catalyst for hydrogen-rich gas

Xiao Lv, Jun Xiao†, Tingting Sun, Xiaodong Huo, Min Song, and Laihong Shen

Key Laboratory of Energy Thermal Conversion and Control of Ministry of Education,
School of Energy and Environment, Southeast University, Nanjing, China
(*Received 5 June 2017 • accepted 15 October 2017*)

Abstract−Tar is a barrier to limit the development of biomass gasification. Catalytic steam reforming experiments using α-methylnaphthalene (MNP) as a model tar compound were carried out in the two-stage reactor system (TSR). Based on response surface methodology, the effects of TSR temperatures and the molar ratio of steam to carbon (S/C) on MNP reforming performances were analyzed using the Li-modified Ni-based catalyst (NBC). The results show that the proper introduction of H_2 is able to improve significantly the MNP conversion, specially at lower temperatures. Furthermore, it is more appropriate for the modified catalysts by Li and Mg to be loaded in the first reactor due to their significant promotion to hydrocracking reactions, and it is favorable to place the Ni/Al catalyst in the second reactor for H_2-rich gas. Additionally, the carbon deposition resistance of the NBC modified by Li exhibits better than that of the NBC modified by Mg.

Keywords: Steam Reforming, Ni-based Catalyst Modified by Li, Hydrogen, Tar, α-Methylnaphthalene

INTRODUCTION

Biomass, being environmental friendly and abundant in reserve, is considered as a promising green energy, and its utilization has great significance to ease the energy crisis and reduce environmental pollution [1-3]. Biomass steam gasification at lower temperature is an efficient method to produce H_2-rich gas from the organics in it, which is of broad prospect [4,5]. However, one of the main problems lies in the high content of tar in the produced gas during the steam gasification process of biomass.

The number of tar components generated during biomass gasification can range from hundreds to thousands, depending on the nature of the biomass as well as the reaction conditions [6]. Unless successfully removed, tar tends to block pipelines, inhibit engine operation, reduce overall conversion efficiency, etc. Steam reforming, which eliminates tar catalytically and produces additional H_2 at lower temperatures, is considered to be the most efficient method for tar removal [7,8].

Considering the complexity of tar components, various model compounds of tar, such as cyclohexane, benzene, toluene, naphthalene, n-hexane, etc. [9-11], are selected to study the reforming performance instead of biomass tar. Generally, the higher the aromatic cycle content is, the lower the reaction rate is, whereas naphthalene, which shows the least reactivity of all the studied compounds, is an exception to this rule and is considered as the most stable model compound of biomass tar [12,13].

Devi et al. [14] studied the steam reforming performance of biomass tar using naphthalene as model compound, and reported that the heating pretreatment of olivine enhanced the conversion efficiency from 50% to 62% at 900 °C, which was relatively low. Michel et al. [15] reported that the water pretreatment of Ni/Olivine catalyst was able to raise the conversion efficiency of α-methylnaphthalene from 30% to 70% at 900 °C, which was still limited. These studies indicated that higher temperatures were necessary for the efficient conversion of naphthalene.

As for the catalysts employed in steam reforming, various catalysts, such as Ni, Co, Pt, dolomite, and olivine, have been studied to improve tar conversion effect, where Ni-based catalysts (NBC) have attracted great attention due to their higher activity and lower cost [11]. However, the NBC tends to be inactivated due to sintering, carbon deposition and the loss of active Ni^0 especially at relatively poor reaction conditions; and lower catalytic activity is also shown by NBC when it is employed for the reforming of comparatively stable compounds [16]. Additionally, the Ni-based catalysts have toxic problems as they are disposed; thus the use of Ni-based catalyst would cause adverse environmental impact.

To promote the catalytic activity and stability of NBC, the catalyst modifications have been developed by different metals, including rare earth metals and alkali earth metals, to enhance catalytic activities and suppress carbon deposition. Li et al. [17] and Miyazawa et al. [18] reported that by introducing CeO_2 to NBC, it could supply oxygen atoms to the absorbed species on Ni surface, which resulted in higher catalytic activity and lower coke formation. Dieuzeide et al. [19] noted that the doped Mg in Ni-Mg/Al_2O_3 promoted both carrier basicity and Ni dispersion, showing increased catalytic performances during the steam reforming of glycerol. Yang et al. [20] revealed through their work that the modification of Mg was favorable for increasing the catalytic activity and stability of NBC, and the catalytic activity of the modified catalyst was also improved during the steam reforming of α-methylnaphthalene.

†To whom correspondence should be addressed.
E-mail: jxiao@seu.edu.cn, jxiaoseu@163.com

Several researchers also studied the effect of the modification of alkali metals on NBC during tar reforming, which exhibited enhanced performance to a certain extent. Qi et al. [21] and Kuchonthara et al. [22] showed that K-promoted Ni-catalyst exhibited a higher activity and stability compared to non-promoted Ni-catalyst for steam reforming of methanol and biomass tar. Osaki et al. [23] introduced K to Ni/Al_2O_3 during the reforming process of CH_4, indicating that potassium played a role in dividing the Ni surface into smaller ensembles and, thereby, suppressed carbon deposition. Kong et al. [24] clarified that the NBC modified by Li and La also showed better resistance of carbon deposition and stability during the steam reforming process of toluene. However, more attention was focused on potassium species instead of lithium, and fewer studies of alkali-modified NBC on heavy tar were carried out.

On the other hand, the reforming at lower temperatures contributes to the reduction of energy consumption and carbon deposition as the conversion of tar is an endothermal process. However, the poor conversion of tar at lower temperatures is still a problem to be solved. Polychronopoulou et al. [8] employed supporting Rh catalysts to purify the H_2-rich gas from the biomass model tar compound of phenol within 575 °C-750 °C, indicating that phenol was efficiently removed with enhanced H_2 concentration. Nevertheless, there is a lack of studies on the effect of H_2-rich atmosphere on the conversion of heavy tar.

The aim of this paper lies in exploring the way to realize the efficient conversion of biomass tar at lower temperatures. Considering that α-methylnaphthalene (MNP) tends to be converted into naphthalene and benzene [21], the selection of MNP as a model tar compound can better reflect the reforming characteristics of biomass tar. To investigate the effect of Li modification on NBC, a series of catalytic reforming experiments were conducted employing the two-stage reactor (TSR). First, to maximize the catalytic activity of the NBC modified by Li for MNP reforming, the influence of reforming temperatures and the molar ratio of steam to carbon (S/C) was studied using the NBC modified by Li, based on response surface methodology. Then, to find a way to reduce the reaction temperature, we investigated the effect of hydrogenation on reforming by introducing H_2 rich atmosphere, realizing efficient conversion of MNP at lower temperatures. In addition, to further study the specific effects of alkali metal and alkaline earth metal modification on Ni-based catalyst, the catalytic reactivity and carbon deposition between the NBCs modified by Li and Mg was also compared.

EXPERIMENTAL

1. Materials

The model tar compound MNP was produced by Aladdin Corporation, America, and its purity was over 96%. The catalysts employed in this paper were all supported by γ-Al_2O_3 (0.3 mm-0.6 mm) and prepared with impregnation method, including the Ni-based catalyst (NBC), the NBC modified by Li and the NBC modified by Mg.

To prepare the NBC, $Ni(NO_3)_2$ aqueous solution, in which $Ni(NO_3)_2{\cdot}6H_2O$ (AR 98.0%, produced by Kelon chemical factory in China) was dissolved in a certain amount of deionized water, was impregnated into γ-Al_2O_3 to achieve the NiO concentration of 20 wt%. After soaking for 20 h, the semi-finished product was dried in an oven at 105 °C. Then, the dried product was calcined in a muffle furnace at 800 °C and 900 °C for 2 h, respectively. At last, the calcined product was reduced at 900 °C in a tube reactor for 1 h under a continuous flow of 20 vol% H_2/N_2 (1 L/min) to obtain the NBC, which was denoted as Ni/Al.

The preparation process of the NBC modified by Li (Mg) was similar to that of Ni/Al, and the differences lie below: First, the aqueous solution contained both $Ni(NO_3)_2{\cdot}6H_2O$ and $LiNO_3$ ($Mg(NO_3)_2{\cdot}6H_2O$). Second, the concentration of Li_2O (MgO) was 2 wt% (10 wt%), determined by our previous study and the literature [24].

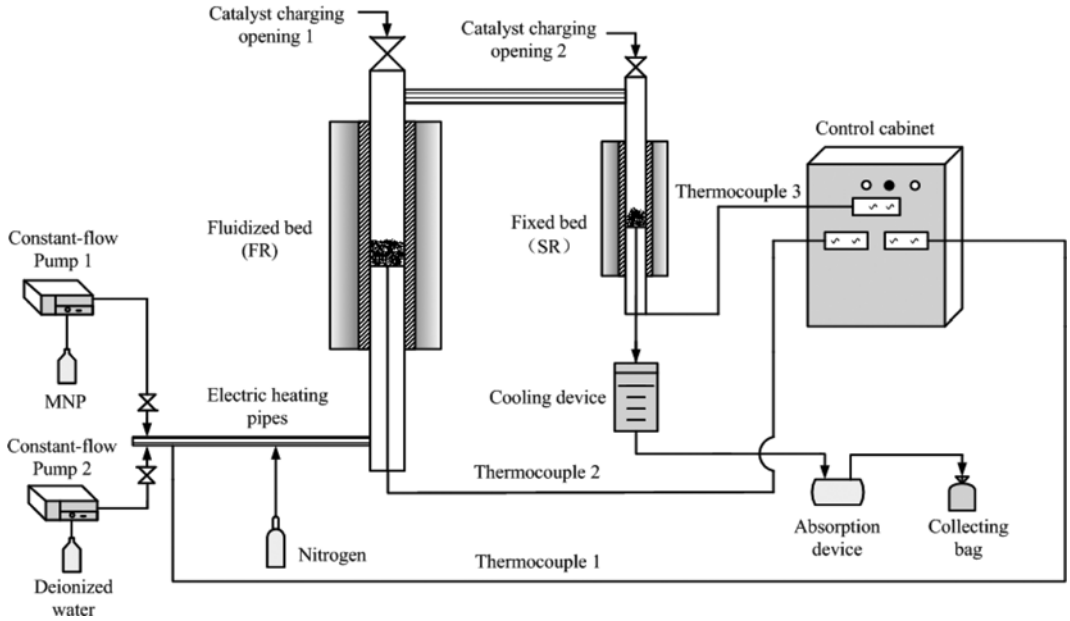

Fig. 1. Experimental system for MNP steam reforming.

Finally, the calcination temperatures were 550 °C for 1 h, 800 °C and 900 °C for 2 h, separately. The employed $LiNO_3$ (AR 99.0%) and $Mg(NO_3)_2{\cdot}6H_2O$ (AR 99.0%) are analytical reagents produced by Kelon Chemical in China. The modified catalysts are denoted as Ni-Li/Al (Ni-Mg/Al).

2. Experimental System

The experimental system for steam reforming of MNP is shown in Fig. 1. The whole system consists of reaction system, steam generating unit, cooling and collecting devices, and electric heating control system. The reaction system is comprised of the TSR, where the fluidized bed reactor (31 mm internal diameter, 600 mm height) is used as the first reactor (FR), and the fixed bed reactor (20 mm internal diameter, 400 mm height) is employed as the second reactor (SR). In a typical run, the TSR are initially heated to required temperatures, and the whole system is purged by nitrogen during the heating process, ensuring the inert atmosphere. Then, 5 g and 4 g catalysts are fed into FR and SR separately from the upper charging openings. When the whole system is stable enough, MNP and steam are continuously fed. The reaction process lasts for about 5 h. The flow rates of nitrogen and MNP are 400 ml·min^{-1} and 0.03 g·min^{-1}, respectively, the flow rate of water is determined by the different molar ratios of steam to carbon (S/C). At these flow rates, the catalyst particles in FR are in the fluidized state. The vapors of MNP and water are generated by injecting MNP and deionized water to the electric heating pipes, using LabAlliance 110SF chromatographic pump and HLB-02/40 constant-flow pump, separately. The temperature of the electric heating pipes is controlled at 300 °C by the electric heating control system. The raw product gas is purified by passing through absorption and cooling devices, which consist of water condenser pipe and a bottle of allochroic silicagel. Then the purified product gas is collected in bags and analyzed by the NGA2000 gas analyzer of EMERSON Company, America.

3. Experimental Scheme

Response surface methodology (RSM), a statistical method for modeling and optimizing a process based on multivariant non-linear model, has been widely utilized in optimizing the operating variables. A mathematical model that best fits to the experimental data was developed. Using this model, the response results can be predicted for various operating variables without experiment, and the optimums of operating variables that generate a maximum or minimum response can be obtained [25,26].

In this study, a series of preliminary experiments were conducted to compare the catalytic activities of Ni/Al, Ni-Li/Al and Ni-Mg/Al. Then, the most effective catalyst was employed for further experiments. The experimental scheme was designed based on Box-Behnken design (BBD) and conducted by Design-Expert software. The temperatures of FR (T_1) and SR (T_2) as well as the S/C were selected as operating variables to study the response variables of carbon conversion efficiency (X_C) and hydrogen yield (R_{H2}). Therefore, 15 experiments with 3 factors and 3 levels were carried out to investigate the synergistic influence of the experimental conditions on MNP steam reforming performances. Specifically, the temperatures of TSR were 750 °C, 825 °C and 900 °C while S/C varied among 6, 9 and 12.

4. Data Processing

Considering the reforming process is a continuous reaction, the responses are determined by the stabilizing stage. Carbon conversion efficiency can be defined as follows:

$$X_C=(n_{CO2}+n_{CO}+n_{CH4})\cdot MW_C\cdot 100/W_C \quad (1)$$

in which X_C is the carbon conversion efficiency (%), n_i is the mole number of gas i (CO, CO_2 and CH_4) produced from one kg MNP (mol/kg-tar), MW_C is the molar mass of carbon (g/mol) and W_C is carbon content per kg MNP (g/kg).

The main products of MNP steam reforming are CO, CO_2, CH_4 and H_2, and hydrogen yield can be obtained by the following formula:

$$R_{H2}=V_{H2}/22.4/m \quad (2)$$

where R_{H2} is the hydrogen yield (mol/kg-tar), V_{H2} is the volume of produced hydrogen under normal temperature and pressure (L), m is the mass of MNP introduced in a certain time (kg).

Gas concentrations of CO, CO_2, CH_4 and H_2 are stated as follows:

$$C_{ni}=n_i/(n_{CO}+n_{CO2}+n_{CH4}+n_{H2}) \quad (3)$$

in which C_{ni} is the concentration of gas i (CO, CO_2, CH_4 and H_2) in the main gas products.

5. Main Reactions in Reforming Process

During the steam reforming of MNP, the main reactions include hydrocracking reaction, dry and steam reforming reactions, thermal cracking reaction and water gas shift reaction, which are shown below.

$$2{\cdot}C_{11}H_{10}+9{\cdot}H_2\rightarrow C_{10}H_8+C_6H_6+6{\cdot}CH_4 \quad (R1)$$

$$C_{10}H_8+7{\cdot}H_2\rightarrow C_6H_6+4{\cdot}CH_4 \quad (R2)$$

$$C_xH_y+x{\cdot}H_2O\rightarrow x{\cdot}CO+(x+y/2){\cdot}H_2\ (x=6,\ 10\ \text{or}\ 11) \quad (R3)$$

$$C_xH_y+2x{\cdot}H_2O\rightarrow x{\cdot}CO_2+(2x+y/2){\cdot}H_2\ (x=6,\ 10\ \text{or}\ 11) \quad (R4)$$

$$C_6H_6+6{\cdot}CO_2\rightarrow 12{\cdot}CO+3{\cdot}H_2 \quad (R5)$$

$$C_mH_n\rightarrow C+H_2+CH_4+\cdots \quad (R6)$$

$$CO+H_2O\rightarrow H_2+CO_2 \quad (R7)$$

6. Catalyst Characterization Methods

In this study, X-ray diffractometry (XRD) was employed to gain insight into the metal phases of Ni/Al, Ni-Li/Al and Ni-Mg/Al (D8-discover X-ray diffraction instrument, made by Bruker, Germany) at a setting of 40 kV and 30 mA (Cu K_α radiation). The scanning range of 2θ was 10°-90° with the rate of 10°/min.

Brunauer-Emmett-Teller (BET) measurement was used to study the specific surface areas and pore properties of Ni/Al, Ni-Li/Al and Ni-Mg/Al (ASAP2020 Specific surface area and pore analyzer, made by Micromeritics Instrument Corporation, America). Measurement ranges were over 0.0005 m^2/g for specific surface area, 3.5 A-5000 A for pore size and over 0.0001 cm^3/g for pore volume.

Thermogravimetric Analysis (TG) was used to investigate the content of deposited carbon in used catalysts (STARe System Thermal analyzer, made by Mettler Toledo, America). The heating rate was 10 °C/min under air atmosphere.

X-ray photoelectron spectroscopy (XPS) was performed to study the species and fractions of the deposited carbon in used catalysts (PHI Quantera II spectrometer equipped with Al K_α radiation,

Japan). The binding energies were calibrated internally by adventitious carbon deposit C (1s) at 284.6 eV (accuracy within ±0.1 eV). The sensitivity was over 15kcps while the energy resolution was less than 0.60 eV.

Temperature-programmed reduction (TPR) analysis was carried out to investigate the reduction properties of catalysts with a thermal conductivity detector (TCD) (FINESORB-3010 Temperature programmed chemical characterization instrument, made by Finetec Instruments, China). Prior to the analysis, catalysts were pretreated at 200 °C for 65 min in Ar flow to clean the surface and cooled to room temperature. After the pretreatment, a 10 vol% H_2/Ar gas was passed through the sample at 20 ml/min and the temperature was raised to 900 °C at a heating rate of 10 °C/min.

RESULTS AND DISCUSSION

1. Catalyst Characterization

1-1. BET Analysis

The specific surface and pore properties of Ni/Al, Ni-Li/Al and Ni-Mg/Al are presented in Table 1. Compared to the supporter γ-Al_2O_3, the specific surface areas of different catalysts decrease to a certain extent while the pore volumes barely change. Besides that, the pore sizes increase obviously. It can be seen from Fig. 2(a) that the N_2 adsorption and desorption isothermal plots of these catalysts exhibit a typical IV type isotherm, which can be attributed to the mesoporous feature, and more than 80% of pores exist in the range of 2 nm-50 nm. As shown in Fig. 2(b), the maximum dV/dW of the catalysts decreases, indicating the range of pore size dis-

Table 1. Results of BET characterization

Samples	Specific surface area m^2/g	Pore volume cm^3/g	Pore size nm
γ-Al_2O_3	105.14	0.39	12.70
Ni/Al	67.70	0.39	22.99
Ni-Li/Al	62.42	0.43	27.39
Ni-Mg/Al	73.80	0.42	22.65

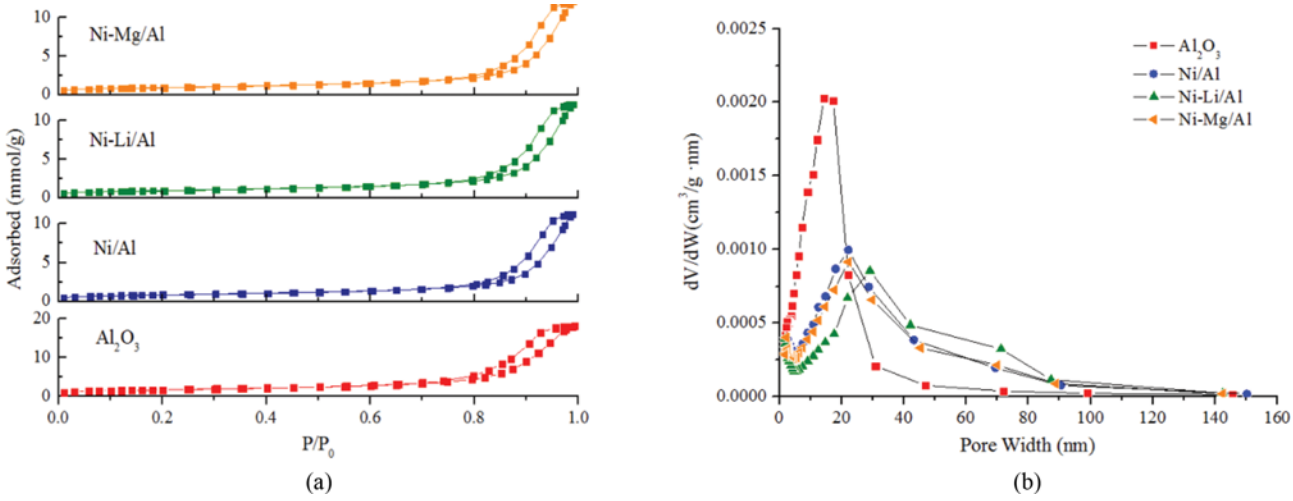

Fig. 2. Pore size distributions of catalysts and supporter. (a) Isothermal adsorption and desorption plots, (b) pore size distributions of catalysts.

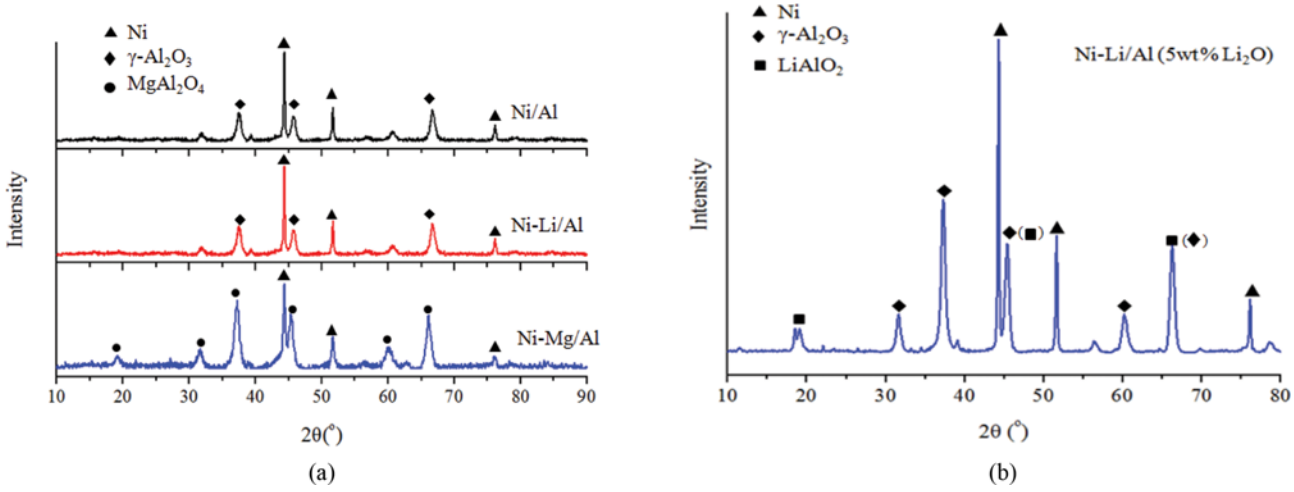

Fig. 3. XRD patterns of the catalysts. (a) XRD patterns of the experimental catalysts, (b) XRD pattern of the Ni-Li/Al with 5 wt% Li_2O.

tribution is increased and the corresponding pore size is enlarged. Because of the loaded active components and the calcining process, small-size pores decrease in contrast to the increase of large-size pores, reducing the surface area without causing any obvious change to the pore volume.

1-2. XRD Analysis

The XRD patterns of Ni/Al, Ni-Li/Al and Ni-Mg/Al are illustrated in Fig. 3(a). To start with, remarkable peaks of Ni (2θ= 44.5°, 51.8° and 76.4°) and γ-Al_2O_3 (2θ=66.6°, 45.7° and 37.6°) can be seen in all the patterns. As we have known, $NiAl_2O_4$ is the main phase of Ni while Mg and Li exist in the forms of $MgAl_2O_4$ and $LiAlO_2$, respectively, before reduction [20,27]. It shows that the crystallization of $NiAl_2O_4$, $MgAl_2O_4$ and $LiAlO_2$ formed at the surface of γ-Al_2O_3 tends to inhibit its transition to other phases such as α-Al_2O_3, etc., which is consistent with the study of Derazet al [27]. In addition, significant peaks of $MgAl_2O_4$ are observed in Ni-Mg/Al, which is the major phase of Mg in Ni-Mg/Al, conforming to the research of Yang [20]. However, the differences between the phases of Ni/Al and Ni-Li/Al are negligible, which may be due to the lower concentration of Li_2O as well as the reduction process. Kong et al. [24] reported that with the content of Li in LiLaNi/Al enhanced to 4 wt%, the phase of $LiAlO_2$ (2θ=18.7°, 45.1° and 66.8°) started to appear. To verify the form of existence of $LiAlO_2$, Ni-Li/Al with the content of Li_2O increasing to 5 wt% is also characterized in Fig. 3(b). As shown, the phase of $LiAlO_2$ is observed, which explains the disappearance of Li in Fig. 3(a) due to its low concentration.

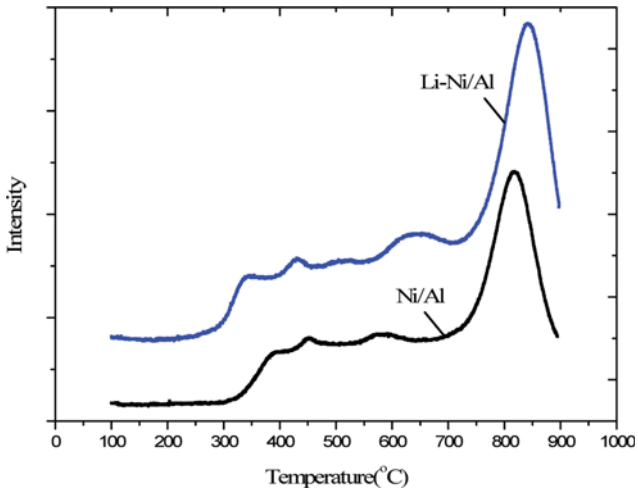

Fig. 4. TPR-H_2 of the catalysts.

1-3. TPR Analysis

The results of the H_2-TPR analyses for Ni-Li/Al and Ni/Al are reported in Fig. 4. For Ni/Al, a small peak is shown at about 450 °C, which can be ascribed to the reduction of NiO [28,29]. By Li modification, this peak shifts to a lower temperature of 430 °C, clarifying that the redox property of Ni-Li/Al is enhanced. Furthermore, when the temperature is above 550 °C, a weak peak at 580 °C and an intense peak at 815 °C are observed for Ni/Al, which can be assigned to the formed $NiAl_2O_4$ spinel with different degrees of

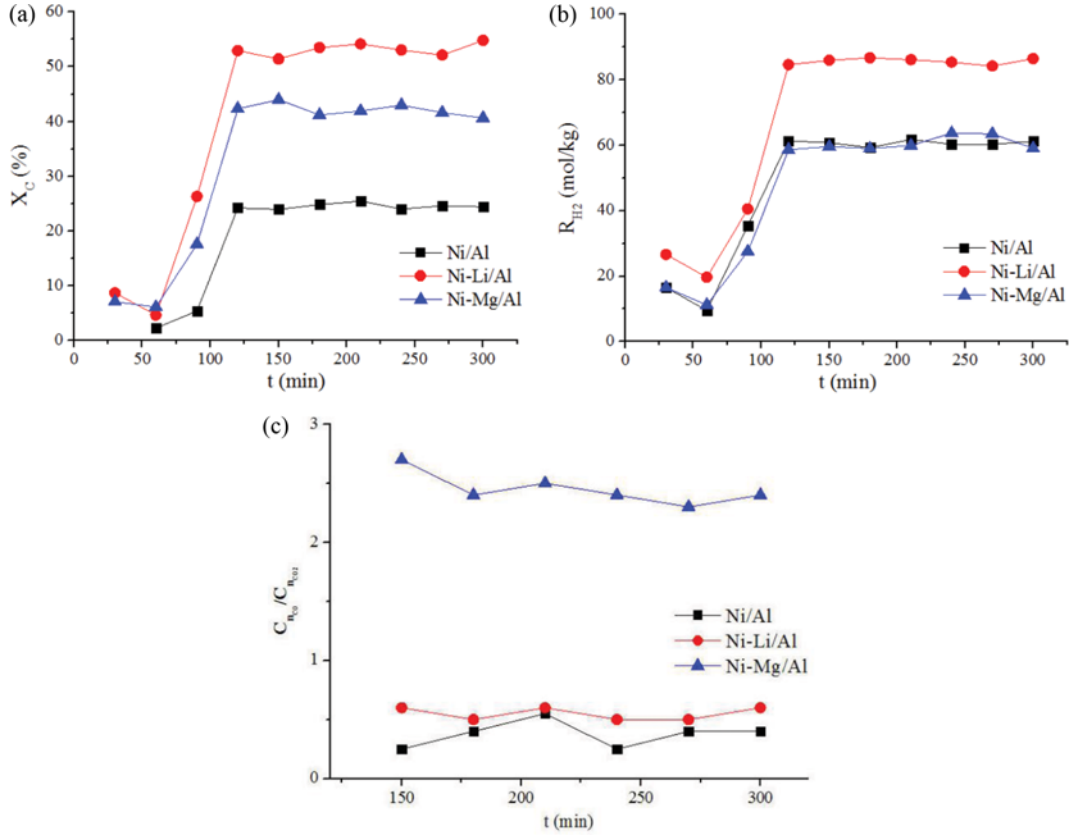

Fig. 5. Reaction processes of preliminary experiments (T_1=T_2=850 °C, S/C=9). (a) X_C, (b) R_{H2}, (c) $C_{n_{CO}}/C_{n_{CO2}}$.

crystallinity [28,30]. With respect to Ni-Li/Al, the two corresponding reduction peaks are transferred to 650 °C and 840 °C, respectively, whose temperatures and intensities are both enhanced compared to Ni/Al. As for $NiAl_2O_4$, higher peak temperatures indicate higher crystallinity, and the formed spinel structure of Ni contributes to its high dispersion on the support surface [28,30], improving the catalytic activity of Ni-Li/Al as a result.

2. Preliminary Experiments

To compare the catalytic performance of Ni/Al, Ni-Li/Al and Ni-Mg/Al during the steam reforming of MNP, three preliminary experiments using the same catalyst in TSR were carried out under the condition of T_1=T_2=850 °C, S/C=9. The results as well as reaction processes are presented in Fig. 5.

As shown in Fig. 5(a) and Fig. 5(b), X_C follows the decreasing order of Ni-Li/Al>Ni-Mg/Al>Ni/Al while R_{H2} shows the trend of Ni-Li/Al>Ni-Mg/Al≈Ni/Al, indicating that the modified catalysts are favorable to the steam reforming of MNP and the effect of Ni-Li/Al is more remarkable. In addition, the three experiments are able to enter stable phases only after 100 min, which can be attributed to the fact that hydrocracking reactions (R1, R2) are limited until appropriate H_2 is available [20]. The initial H_2 comes mainly from the slight steam reforming reaction (R3), and this is further confirmed by the decreasing trend of R_{H2} within the first 60 min.The higher catalytic performance of Ni-Li/Al may be ascribed to the fact that Li enhances H_2 adsorption to facilitate hydrocracking, which is due to the increased nickel electronic density brought by the added alkali metals for their electron donor character [31]. On the other hand, Li and Mg are able to promote the even dispersion of Ni so that the catalytic performance of reforming reactions (R3, R4) is improved. And the basic sites of Ni/Al are enhanced by Li and Mg modification, facilitating CO_2 adsorption performance and dry reform reaction (R5) as a result [29,31].

Furthermore, Fig. 5(c) illustrates that the ratio of $C_{n_{CO}}$ to $C_{n_{CO2}}$ for Ni-Mg/Al is much higher than that for Ni/Al and Ni-Li/Al. It can be learned that the employment of Ni-Mg/Al raises the yield of CO much higher than that of Ni-Li/Al. This is because the basic site activity and CO_2 adsorption performance of Ni-Mg/Al are higher than those of Ni-Li/Al due to the higher amount of Mg loaded.

3. Response Surface Experiment Results

According to the above conclusions, the most effective catalyst Ni-Li/Al is employed for further experiments, based on the response surface methodology. Experimental design and the corresponding results are shown in Table 2.

3-1. Establishment of Response Surface

Based on our early study on biomass steam gasification for hydrogen-rich gas using RSM [32], multiple regression analysis is car-

Table 2. Experimental conditions and results

Case	T_1 °C	T_2 °C	S/C	X_C %	R_{H2} mol/kg-tar
1	750	825	12	23.9	44.0
2	750	750	9	18.2	31.7
3	750	900	9	31.7	59.2
4	750	825	6	15.6	28.0
5	825	825	9	48.4	67.9
6	825	825	9	47.6	66.2
7	825	900	12	58.3	83.8
8	825	900	6	35.2	55.9
9	825	825	9	47.7	67.1
10	825	750	12	32.7	55.9
11	825	750	6	29.1	36.4
12	900	750	9	59.2	84.8
13	900	825	6	51.1	74.1
14	900	900	9	73.7	108.2
15	900	825	12	69.4	101.1

Table 3. Variance analysis of the response models

Response variables	X_C			R_{H2}		
	Coefficient	Sum of squares	*p*-Value	Coefficient	Sum of squares	*p*-Value
Model		4489.2	0.000		9497.5	0.000
A	20.50	3362.0	0.000	0.29	6305.6	0.000
B	7.46	445.5	0.000	0.36	1441.8	0.000
C	6.66	355.1	0.000	−10.05	1225.1	0.000
AB	0.25	0.3	0.518	0.00	5.1	0.105
AC	2.50	25.0	0.001	0.01	36.6	0.003
BC	4.88	95.1	0.000	0.02	21.6	0.009
A^2	−0.51	1.0	0.229	0.00	65.3	0.000
B^2	−1.69	10.5	0.006	0.00	0.0	0.930
C^2	−7.39	201.5	0.000	−0.82	368.9	0.000
Residual		2.6			6.5	
Lack-of-fit		2.2	0.211		4.7	0.387
Total		4491.8			9504	
R^2	0.999			0.999		
Adj-R^2	0.998			0.998		
Pred-R^2	0.992			0.992		
Adeq precision	99.6			99.5		

ried out using Design-Expert software for the data in Table 2, and the results are shown in Table 3, where T_1, T_2 and S/C are denoted as A, B and C separately.

On account of the analysis of variance (ANOVA), a number of statistical conclusions can be obtained as follows: (i) *p* values of all the models are far less than 0.01, which indicates remarkable significance and reliability of the models; (ii) the R^2 values of X_C and R_{H2} illustrate that both the models can, respectively, explain 99.9% of changes in the experiments; (iii) Adj-R^2 values are greater than 0.8, further demonstrating the model reliability; (iv) the values of Pre-R^2 for X_C and R_{H2} are reasonably consistent with those of Adj-R^2; (v) lack-of-fit and Adeq precision tests are performed to study

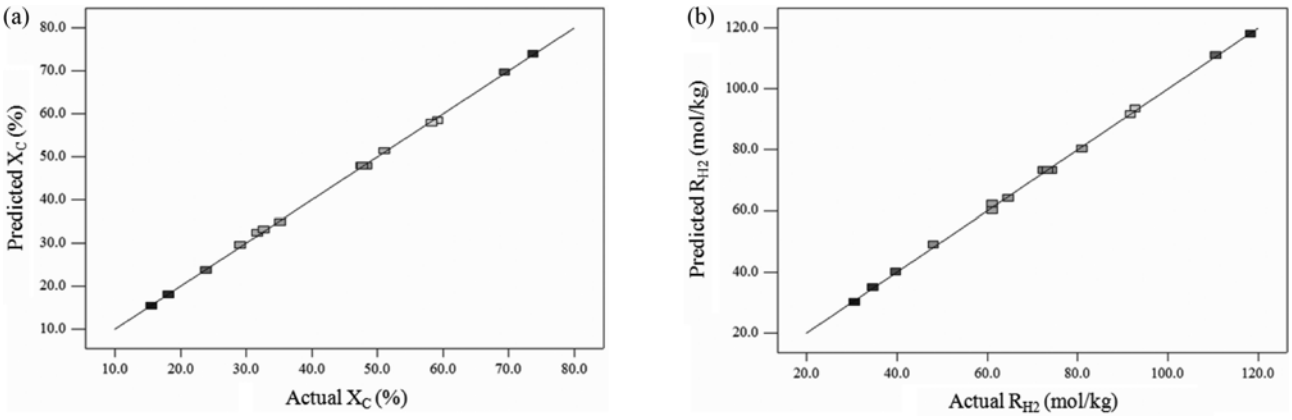

Fig. 6. Prediction accuracy analysis of response models. (a) X_C, (b) R_{H2}.

Table 4. Second-order polynomial equations of X_C and R_{H2}

Response	2nd order polynomial equations
X_C	$47.90+20.50X_1+7.46X_2+6.66X_3+0.25X_1X_2+2.50X_1X_3+4.87X_2X_3-0.51X_1^2-1.69X_2^2-7.39X_3^2$
R_{H2}	$73.37+28.07X_1+13.42X_2+12.38X_3-1.12X_1X_2+3.02X_1X_3+2.32X_2X_3+4.20X_1^2+0.05X_2^2-10.00X_3^2$

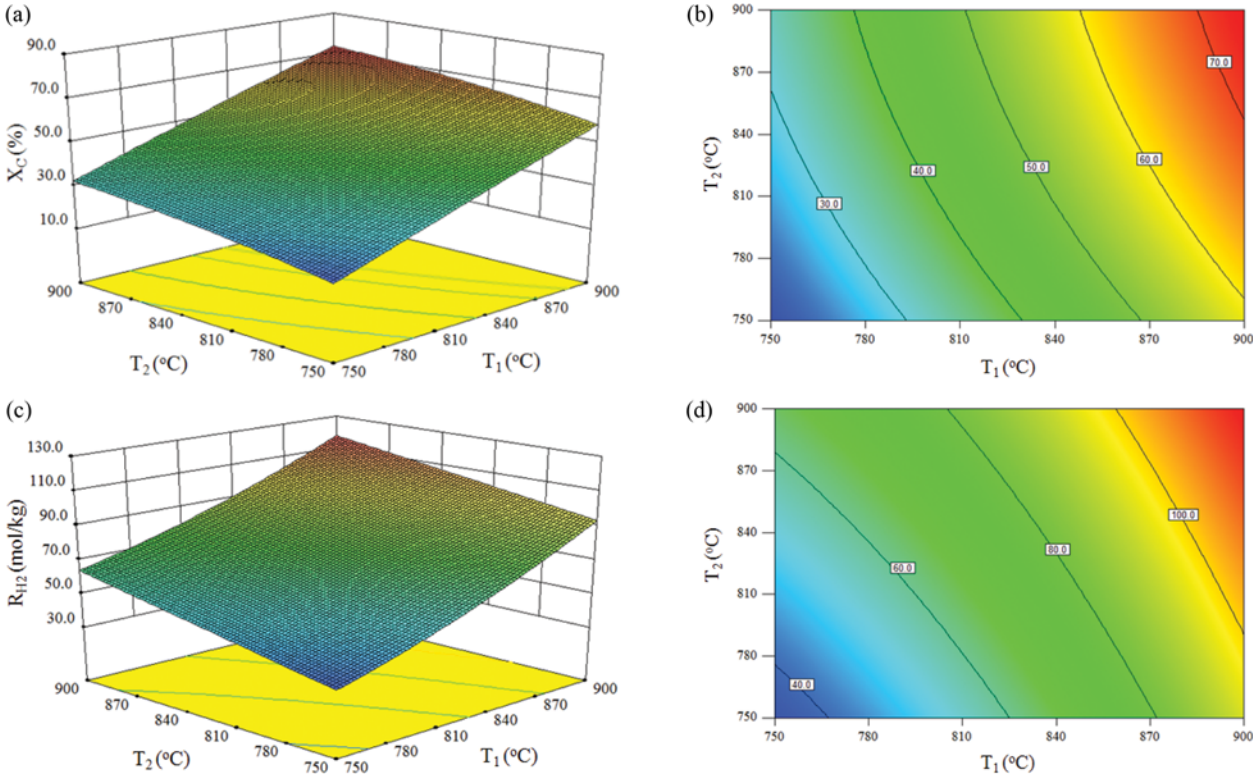

Fig. 7. Effect of T_1 and T_2 on X_C and R_{H2}. (a) X_C response surface, (b) X_C contours, (c) R_{H2} response surface, (d) R_{H2} contours.

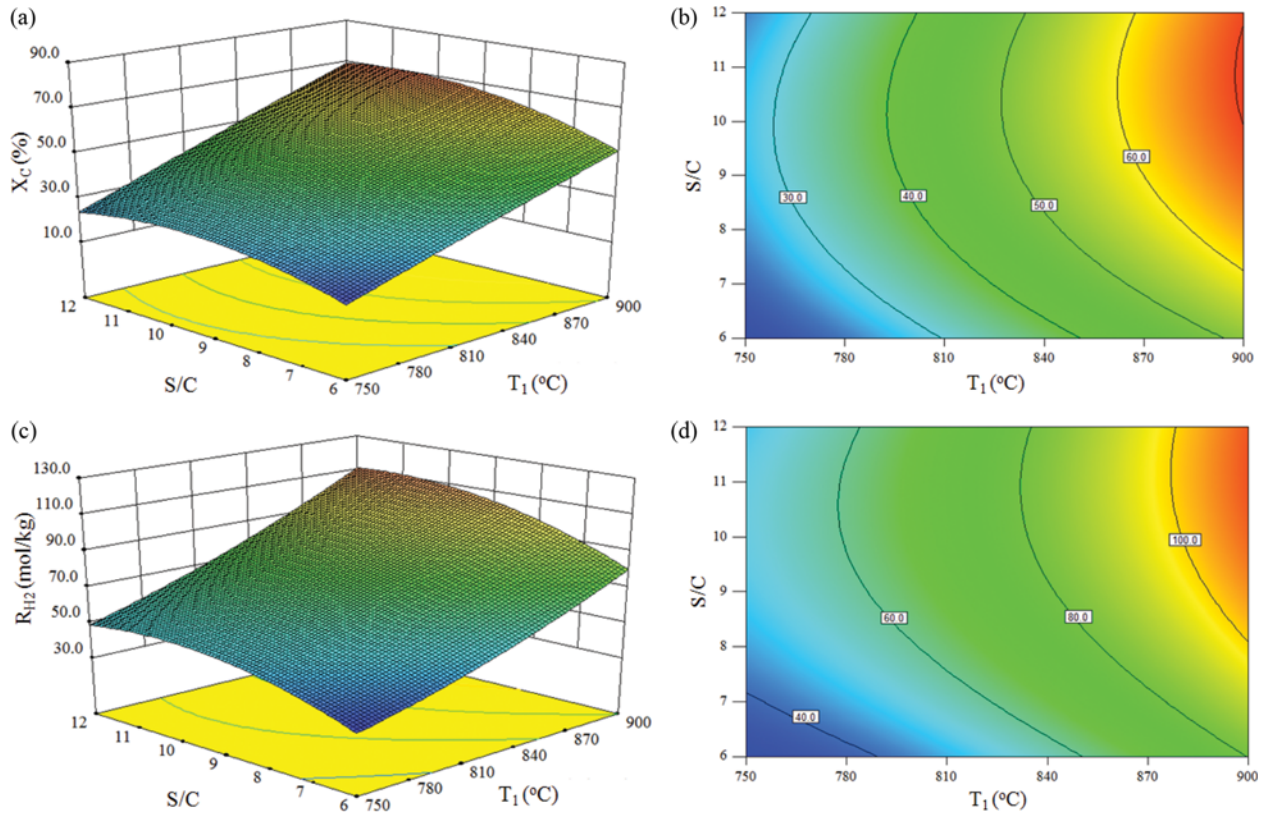

Fig. 8. Effect of T_1 and S/C on X_C and R_{H2}. (a) X_C response surface, (b) X_C contours, (c) R_{H2} response surface, (d) R_{H2} contours.

the impact of noise on signal, where the *p*-values of lack-of-fit are greater than 0.05 and the Adeq precision values are no less than 4, indicating that the two response models are feasible to navigate the design space.

Fig. 6 shows that predicted and actual points are almost distributed on the diagonal closely and randomly, indicating that both response models have high fitting degree.

3-2. Analysis of Response Surface

Based on the data in Table 3, it is assumed that X_1=(A-825)/75, X_2=(B-825)/75, X_3=(C-9)/3, where A is the temperature of FR (°C), B is the temperature of SR (°C), C is S/C. The 2nd order polynomial equations of the two models can be obtained in Table 4.

On the basis of Table 4 and Design-Expert software, contours and response surfaces about the influence of arbitrary two operating variables on X_C and R_{H2} can be achieved. When S/C is 9, the effect of T_1 and T_2 on response variables is illustrated in Fig. 7. This indicates that with T_1 and T_2 increasing, both X_C and R_{H2} show a trend similar to linear growth, and the impact of T_1 is more significant. By derivation of the regression equations, when T_1 and T_2 are 900 °C, X_C and R_{H2} are able to reach their maximum of 73.9% and 107.9 mol/kg-tar, relatively enhanced by 313% and 236% compared with the minimums of 17.9% and 32.1 mol/kg-tar.

During the MNP reforming process, to start with, a slight steam reforming reaction takes place to produce H_2, and the H_2 is consumed rapidly in hydrocracking reactions (R1, R2) afterwards. The hydrocracking products mainly contain naphthalene, benzene and CH_4 [20], which suffer thermal cracking reaction (R6), steam reforming reactions (R3, R4) and water gas shift reaction (R7), and are eventually converted into small-molecule gases. Higher T_1 is beneficial for the initial steam reforming and hydrocracking reactions to be carried out rapidly and efficiently, while the increase of T_2 gives rise to further reforming reactions of the hydrocracking products. The greater significance of T_1 indicates that the temperature of FR is crucial to the overall reforming performance of MNP. In addition, except for prolonging the residence time of product gases, the employment of SR also promotes reforming and water gas shift reactions.

The effect of T_1 and S/C on X_C and R_{H2} is shown in Fig. 8 while T_2 is kept at 825 °C. As can be learned, both X_C and R_{H2} show a trend of first increasing and then decreasing along with the rise of S/C, and the influence of T_1 is more significant. By derivation of the regression equations, when T_1 and S/C are 900 °C and 10, X_C attains its maximum of 70.7%, a relative growth of 356% achieved compared with the minimum of 15.5%. Furthermore, when T_1 and S/C are 900 °C and 11, R_{H2} reaches a maximum of 102.6 mol/kg-tar, relatively increasing by 274% compared with the minimum of 27.4 mol/kg-tar.

The increased content of steam promotes initial steam reforming reactions greatly, which further gives rise to hydrocracking reactions (R1, R2) as well as steam reforming and water gas shift reactions (R3, R4 and R6), ensuring MNP to be converted into H_2-rich gas efficiently and inhibiting carbon deposition in the catalysts. Excess steam, however, may lead to uneven fluidization in FR, lower residence time and reduce temperature in the core reaction

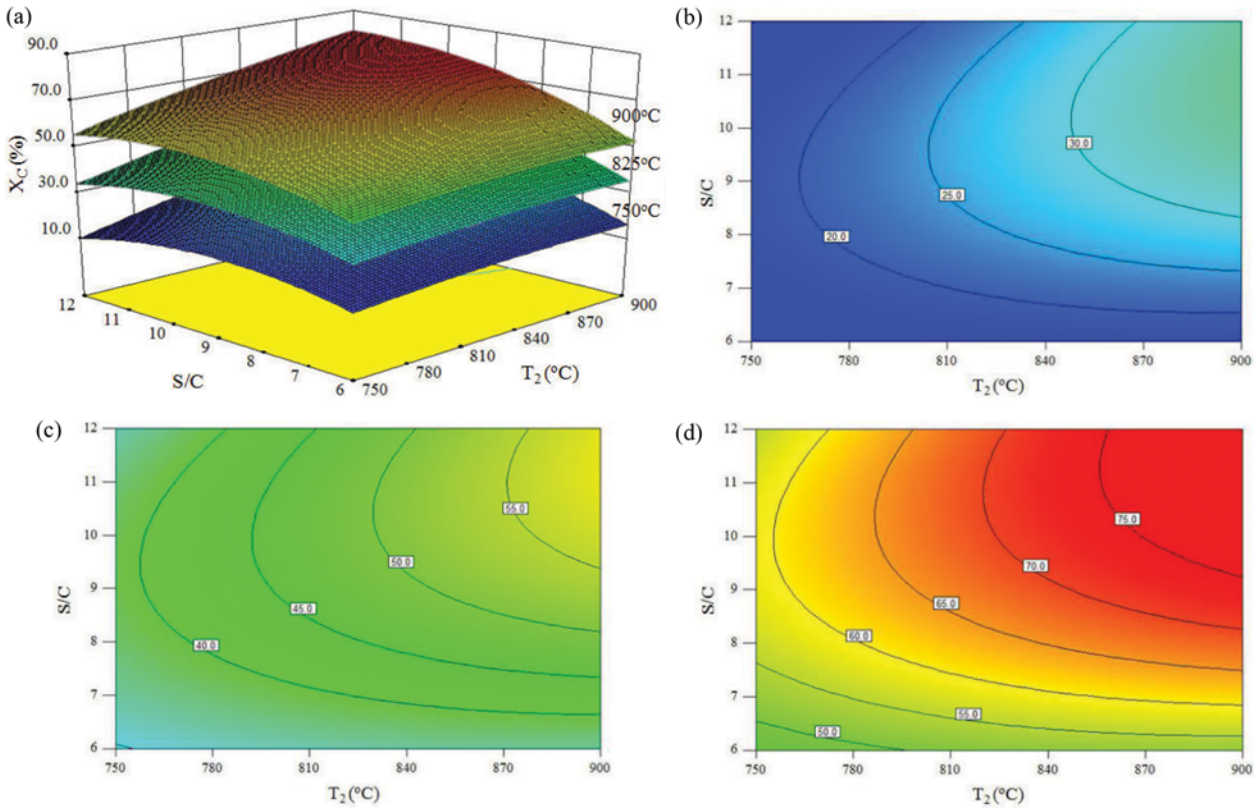

Fig. 9. Effect of T_2 and S/C on X_C with T_1 varying. (a) Response surfaces, (b) 750 °C contours, (c) 825 °C contours, (d) 900 °C contours.

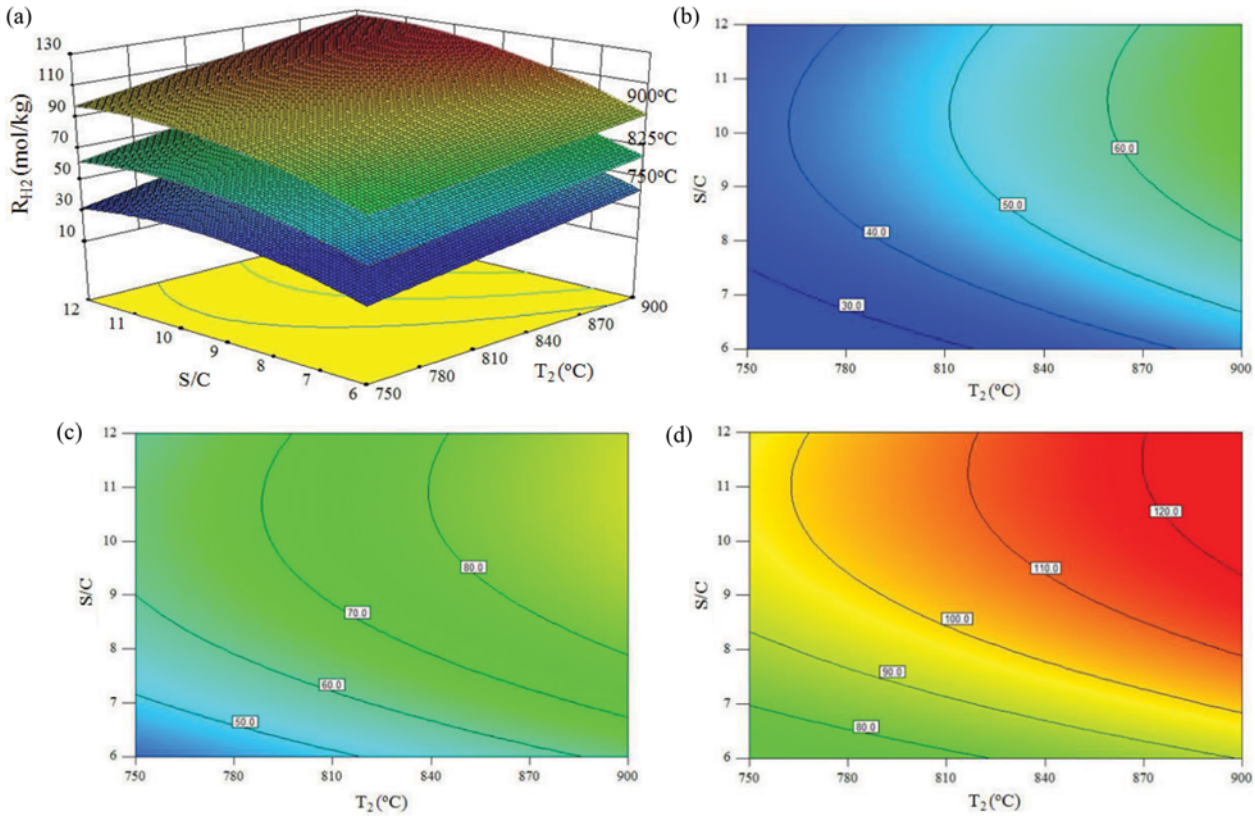

Fig. 10. Effect of T_2 and S/C on R_{H2} with T_1 varying. (a) Response surfaces, (b) 750 °C contours, (c) 825 °C contours, (d) 900 °C contours.

Table 5. Response values from model prediction and experiment

	T_1 °C	T_2 °C	S/C	X_C (%)	R_{H2} (mol/kg-tar)
Prediction	900	900	9	76.1	109.9
Experiment				73.7	108.2

regions [33,34], suppressing the conversion of MNP as a result.

The effect of T_2 and S/C on response variables at different T_1 is revealed in Fig. 9 and Fig. 10. As clarified by the trends of response surfaces, there is little difference between the significance of T_2 and S/C with T_1 varying. By derivation of the regression equations, the maximums of both X_C and R_{H2} can be obtained when T_2 is 900 °C at different T_1, and the corresponding values of S/C follow a trend of first increasing and then decreasing. Specifically, when T_1 is 750 °C, 825 °C and 900 °C, the optimums of S/C are 10, 11 and 9, respectively. This can be attributed to the fact that reactant concentrations have an essential influence on the initial steam reforming reactions when T_1 is relatively low; however, as T_1 is high enough, excess steam may result in reduced partial pressure of H_2, inhibiting hydrocracking reactions. X_C and R_{H2}, therefore, are able to achieve their maximums of 76.1% and 109.9 mol/kg-tar when T_1 and T_2 are 900 °C with S/C reaching 9.

Optimization-numerical module is employed to find the optimums of T_1, T_2 and S/C for the maximizations of X_C and R_{H2} and the prediction conditions are shown in Table 5. The results reveal that the maximum responses can be achieved when T_1 and T_2 are 900 °C with S/C reaching 9, which is in accordance with case 14 in Table 2. The values from prediction and experiment are fairly close, and relative errors of X_C and R_{H2} are 3.3% and 1.6%, respectively. This indicates the rationality of the optimization process.

3-3. Gas Concentration Analysis

Concentrations of CO, CO_2, CH_4 and H_2 in the major gas products are shown in Fig. 11, where the case numbers are consistent with those in Table 2. The results indicate that $C_{n_{CO}}$ fluctuates within the range of 5%-10% while $C_{n_{CO2}}$ and $C_{n_{H2}}$ wave around 20% and 70%, separately, in different cases. Furthermore, $C_{n_{CH4}}$ is less than 5%. With CO_2 captured, the $C_{n_{H2}}$ is expected to be further enhanced to the considerable level of 87%, which is of rather practical significance.

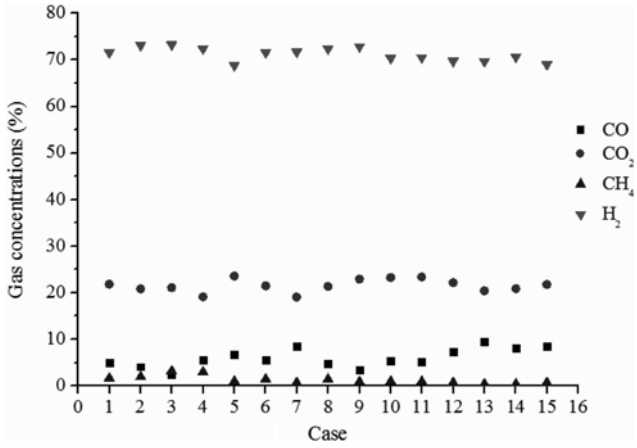

Fig. 11. Concentrations of gas products.

4. Effect of Different Catalysts on MNP Reforming

On account of the preliminary experiments, the catalytic activity of modified catalysts is superior to Ni/Al, and Ni-Mg/Al tends to promote the dry reforming reaction (R5), leading to a large amount of CO generated. In addition, according to our previous study and the literature [33], Ni/Al has significant effect on the steam reforming of light hydrocarbons and water gas shift reaction. Therefore, to further enhance X_C and R_{H2}, the combined methods of Ni/Al, Ni-Li/Al and Ni-Mg/Al were investigated. Under the above optimized condition (T_1=T_2=900 °C, S/C=9), three experiments using different catalysts were carried out. Taking case 14 (Ni-Li/Al in TSR) in Table 2 for comparison, the results of the four experiments are illustrated in Fig. 11, where *catalyst A-catalyst B* means catalyst A is loaded in FR with SR charged with catalyst B.

As shown in Fig. 12(a), Ni/Al-Ni/Al has minor effect on MNP conversion as the initial hydrocracking is vital to the overall reforming performance of MNP, and Ni/Al has little effect on this process. There are no obvious differences between the conversion effects of Ni-Li/Al-Ni/Al and Ni-Mg/Al-Ni/Al, where X_C and R_{H2} are around 85% and 145.1 mol/kg, respectively, and the effects are

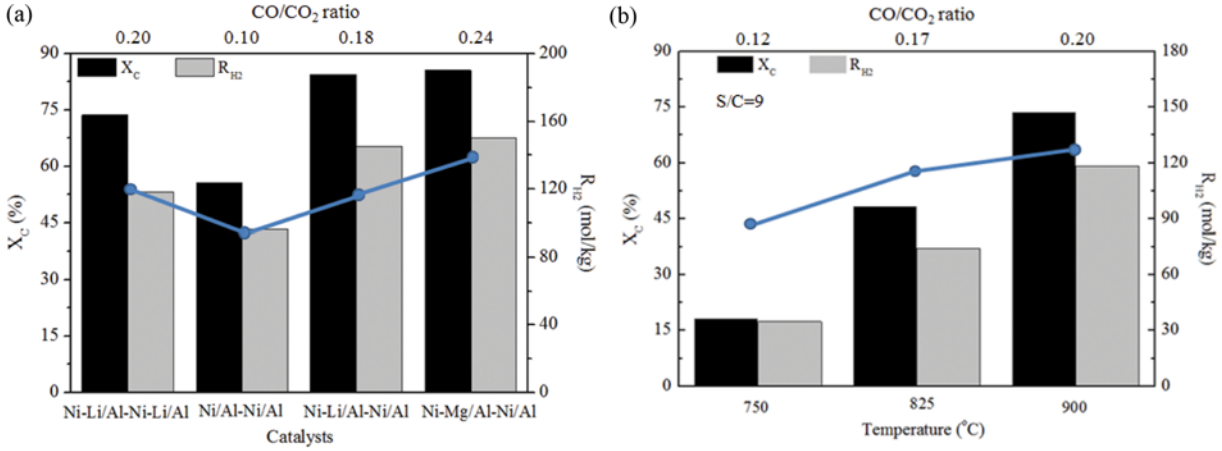

Fig. 12. X_C and R_{H2} of MNP reforming using different catalysts in FR. (a) Effect of catalysts (T_1=T_2=900 °C, S/C=9). (b) Effect of reforming temperatures (Ni-Li/Al-Ni-Li/Al, S/C=9).

significantly improved compared to Ni-Li/Al-Ni-Li/Al, with X_C and R_{H2} increasing by 16.4% and 27.1%, separately. This indicates that Ni-Li/Al and Ni-Mg/Al are able to promote the hydrocracking reactions (R1, R2) to a similar extent, and it is favorable for them to be loaded in FR, where hydrocracking of MNP is the main reaction to produce monocyclic benzene. However, the cracking of monocyclic benzene is harder, and the reforming of benzene is more important in SR [35]. It also can be seen by the R_{H2} and the ratio of CO/CO_2 that the catalytic effect of Ni/Al on steam reforming reactions (R3, R4) and water gas shift reaction (R7) is more prominent, while dry reform reaction (R5) is lower compared with the modified catalysts. Therefore, the Ni/Al in SR is more beneficial to improve R_{H2}. Comparing Fig. 5(a) and Fig. 12(a), it is clear that the gap between Ni-Li/Al-Ni-Li/Al and Ni/Al-Ni/Al is narrowed with temperature rising from 850 °C to 900 °C, indicating that the effect of Ni-Li/Al is more significant especially at lower temperatures.

It is shown in Fig. 12(b) that when Ni-Li/Al is employed in TSR, X_C and R_{H2} almost show a trend of linear growth, and the ratio of CO/CO_2 is also enhanced, with reforming temperature increasing. The enhancement of the ratio of CO/CO_2 can be ascribed to the weakened water gas shift reaction and the strengthened dry reforming reaction at higher temperatures.

Therefore, it is beneficial for the heavy tar, such as naphthalene and α-methylnaphthalene, to use two stage reactors, with Ni-Li/Al promoting hydrocracking in FR and Ni/Al converting the products of hydrocracking into hydrogen-rich gas efficiently in SR.

5. Stability Tests of Catalysts

Stability tests of the Ni-Li/Al and Ni/Al were carried out under the condition of T_1=T_2=900 °C and S/C=9 for 20 h, with Ni-Li/Al and Ni/Al loaded in FR, respectively, and the same amount of Ni/Al placed in SR. The results are shown in Fig. 13. With respect to the Ni-Li/Al, X_C and R_{H2} are separately kept at the averages of 81.2% and 142.8 mol/kg with fewer fluctuations, while the averages are 77.4% and 136.9 mol/kg for Ni/Al. Additionally, the catalytic activity of both Ni-Li/Al and Ni/Al can be recovered when their performance starts to show a trend of decline. Therefore, the catalytic activity and stability of Ni-Li/Al are both superior to Ni/Al.

To evaluate the catalyst strength, the catalysts after the 20 h stability tests were sieved. It was found that the particle sizes of the Ni-Li/Al in FR were maintained within 0.3 mm-0.6 mm, taking up 98.7 wt%, while the proportion for Ni/Al in FR decreased to 87.7 wt%. Furthermore, the particle sizes of the attrited Ni-Li/Al still remained more than 0.2 mm, but about 5.1 wt% of the Ni/Al in FR was reduced to less than 0.2 mm, indicating that the Ni-Li/Al has a higher mechanical strength.

6. Effect of Hydrogenation on MNP Reforming

According to the above conclusions, the overall conversion effect of MNP mainly depends on the initial hydrocracking performance, and the hydrocracking reactions are influenced by H_2 concentration greatly. Considering the H_2 consumed in hydrocracking is majorly derived from the slight steam reforming reaction (R3), hydrogenation is employed so as to improve the reforming effect and reduce the reaction temperatures. For the hydrogenation experiment of MNP reforming, the carrier gas contained 7 vol% or 15 vol% H_2/N_2. Furthermore, Ni-Li/Al was loaded in FR while SR was charged with Ni/Al. Fig. 14 illustrates the effects of H_2 concentration, S/C and the temperatures of TSR on MNP reforming, where the experimental condition without hydrogenation is also involved for comparison. The fed hydrogen was excluded to attain the R_{H2}.

The effect of H_2 concentrations in carrier gas is shown in Fig. 14(a), in which T_1 and T_2 are 900 °C with S/C reaching 9. As shown, the hydrogenation is able to enhance the MNP reforming effect remarkably and the maximums of X_C and R_{H2} attain 95.8% and 176.8 mol/kg-tar separately, indicating that MNP is almost converted into H_2-rich gas completely. In addition, the X_C values in the H_2 concentrations of 7 vol% and 15 vol% are close while the R_{H2} in 7 vol% H_2 is much higher, revealing that the appropriate concentration of H_2 is 7 vol%. This can be due to the excess H_2 making the reaction (R7) equilibrium shift to the left, reducing R_{H2} as a result.

The influence of S/C on MNP reforming is illustrated in Fig. 14(b), where T_1 and T_2 are 900 °C with H_2 concentration kept at 7 vol%. Compared to non-hydrogenation process, the hydrogenation tends to enhance X_C and R_{H2} by 10.3% and 25.5%, respectively when S/C is 9. As S/C decreases to 6, X_C and R_{H2} are further increased to 97.6% and 181.2 mol/kg-tar, respectively. However, the conversion effect is reduced sharply when S/C is 3. This indi-

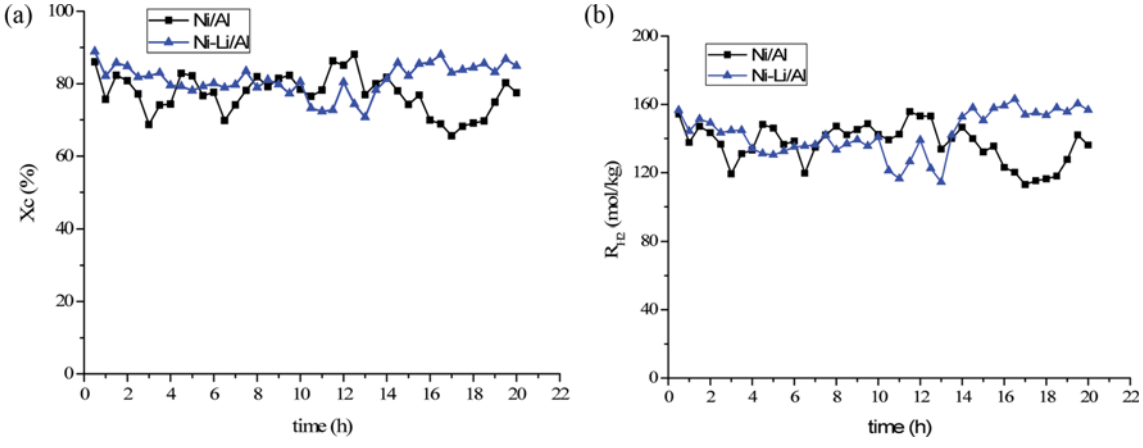

Fig. 13. Stability tests of catalysts. (a) Variation trend of X_C, (b) variation trend of R_{H2}.

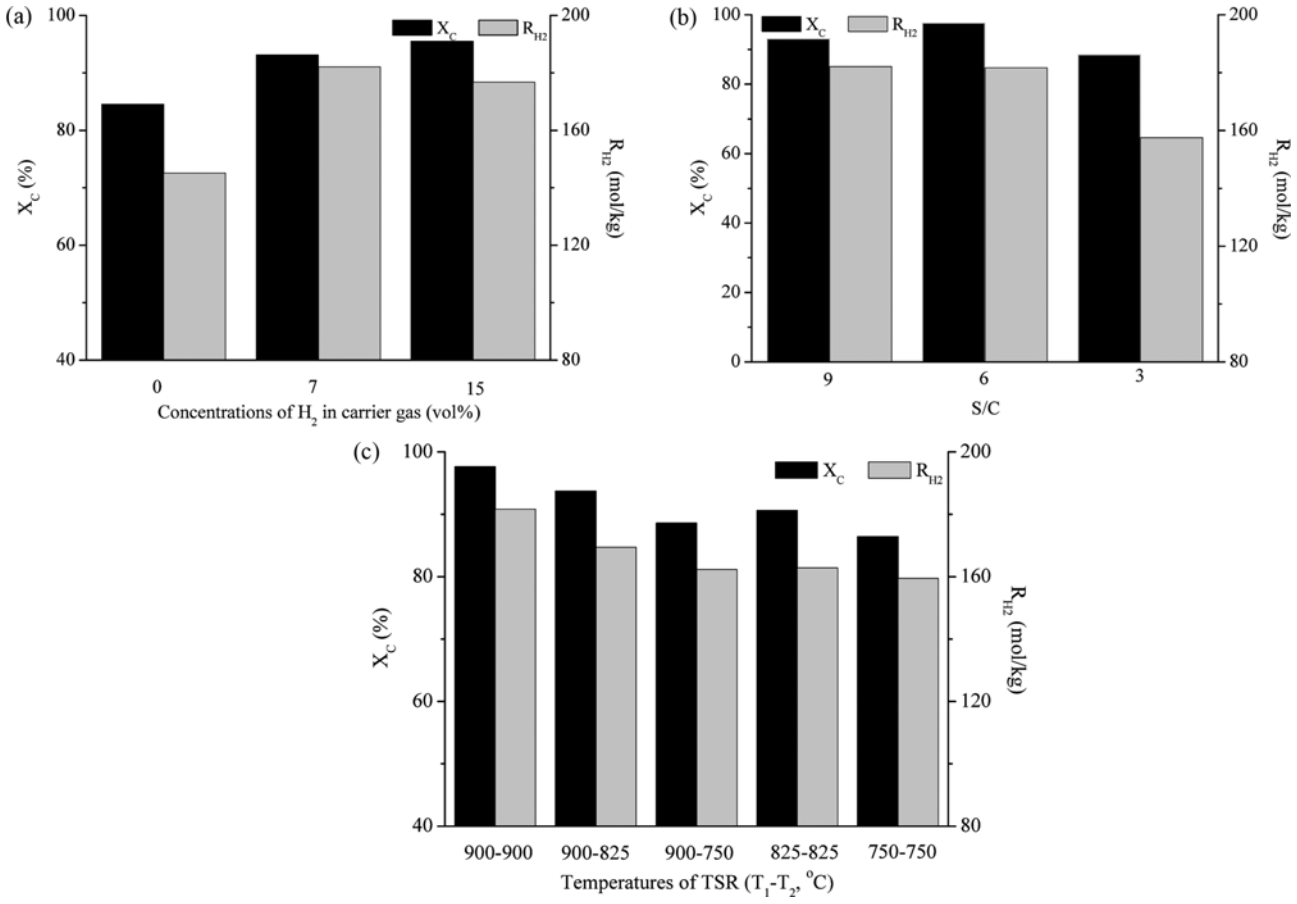

Fig. 14. Effect of hydrogenation on MNP reforming. (a) Effect of concentrations of H_2 in carrier gas (T_1=T_2=900 °C, S/C=9), (b) effect of S/C (T_1=T_2=900 °C, H_2 concentration=7 vol%), (c) effect of T_1 and T_2 (S/C=6, H_2 concentration=7 vol%).

cates that with hydrogenation carried out, there is no need for introducing excess steam to promote the initial steam reforming reaction for hydrogen production, and the moderate reduction of steam is favorable to the increments of reactant partial pressures. Therefore, the suggested S/C is 6.

The effect of reduced T_1 and T_2 is clarified in Fig. 14(c), in which S/C and H_2 concentration are 6 and 7 vol%, respectively. As can be learned, when T_1 and T_2 are reduced to different extents, both X_C and R_{H2} show a trend of decreasing, whereas the conversion effect at lower temperatures is still kept at a relatively high level. Furthermore, even for both reactors at 750 °C, X_C of 86.4% and R_{H2} of 159.5 mol/kg-tar are superior to those of 900 °C-900 °C during non-hydrogenation process, which is increased by 2.2% and 9.9%, respectively. This reveals that the effective steam reforming of MNP can be achieved at lower temperatures by proper hydrogenation.

In summary, the conversion effect of MNP tends to be improved significantly with hydrogenation carried out. As T_1, T_2 and S/C vary in large ranges, X_C and R_{H2} are always maintained at comparatively higher levels, which further indicates the decisive effect of initial hydrocracking on the overall conversion performances of MNP.

7. Carbon Deposition

To study the influence of experimental conditions as well as the modifications of Li and Mg on the carbon deposition behaviors, several used catalysts in TSR are characterized. In this paper, TG is employed to investigate the content of carbon deposition in the used catalysts, while XPS is performed to study the components of the deposited carbon. In the following figures and tables, the loaded catalysts in TSR are denoted as *catalyst A-catalyst B*, which means catalyst A is loaded in FR with SR charged with catalyst B. And the experimental conditions of used catalysts are marked as T_1-T_2-S/C-1 or T_1-T_2-S/C-2, where 1 and 2 represent FR and SR separately.

7-1. TG Analysis

TG analyses of 12 catalyst samples in six conditions are illustrated in Fig. 15. Weight reductions caused by moisture evaporation can be seen in the initial temperature range up to 200 °C for all the samples. Considering the weight increase caused by Ni oxidization, TG analyses of the corresponding fresh catalysts were conducted under the same condition. By subtracting this portion of weight increase, the net weight increases of different samples due to carbon depositions can be obtained, which are shown in Table 6.

For Ni-Li/Al, a remarkable weight loss of 750-900-9-2 is merely observed (around 17 wt%) after 500 °C, indicating that a great amount of carbon is deposited in this sample. In addition, the weight increases of other Ni-Li/Al samples are observed between 400 °C to 700 °C due to the oxidization of Ni in catalysts [36]. As shown in Table 6, the amount of carbon deposition on the cata-

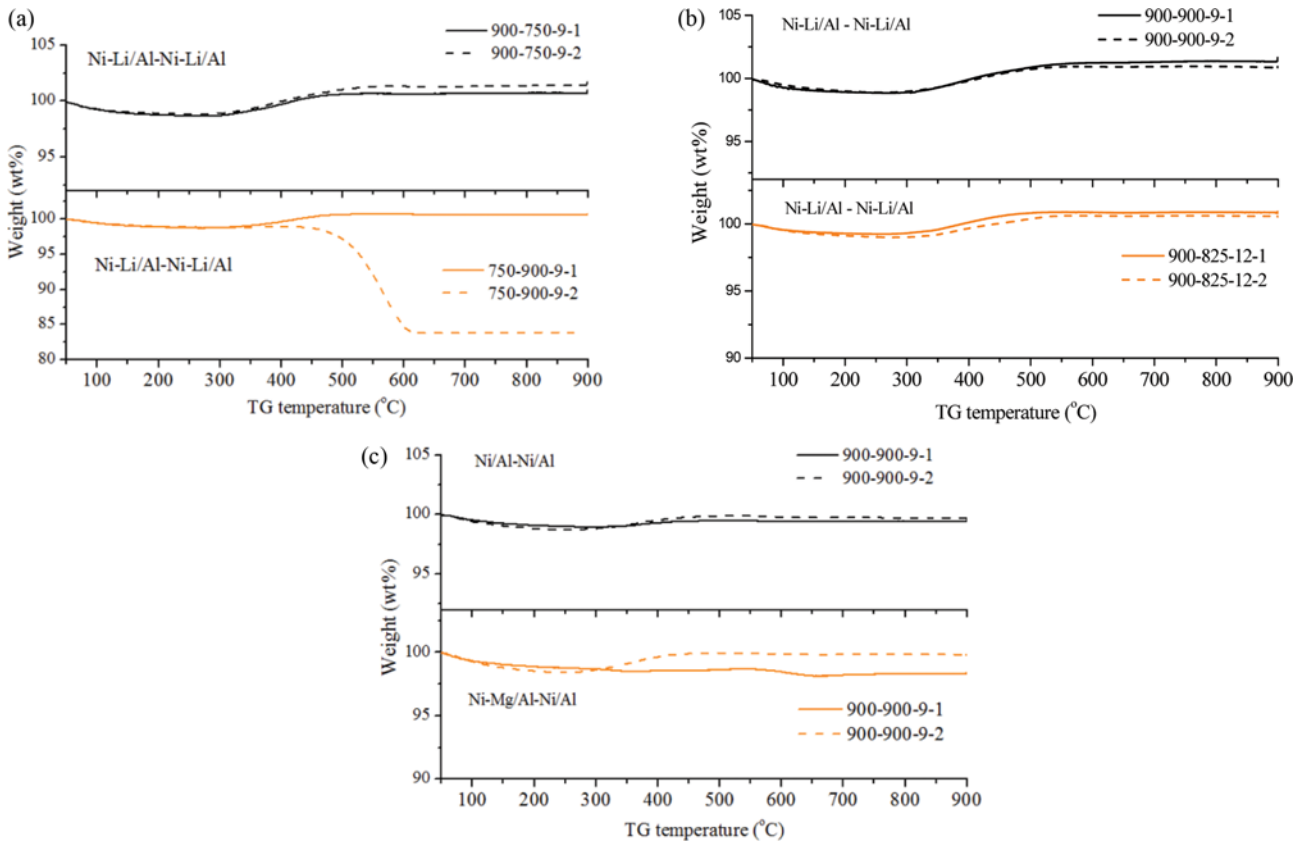

Fig. 15. TG analyses of used catalyst samples. (a) Ni-Li/Al with different temperatures, (b) Ni-Li/Al with different S/C, (c) carbon deposition in Ni/Al and Ni-Mg/Al.

Table 6. Carbon depositions on different catalysts

Catalysts	Experimental conditions of used samples	Carbon depositions on catalysts (g carbon/g catalyst)
Ni-Li/Al	900-750-9-1	0.034
Ni-Li/Al	900-750-9-2	0.019
Ni-Li/Al	750-900-9-1	0.035
Ni-Li/Al	750-900-9-2	0.197
Ni-Li/Al	900-900-9-1	0.037
Ni-Li/Al	900-900-9-2	0.022
Ni-Li/Al	900-825-12-1	0.032
Ni-Li/Al	900-825-12-2	0.029
Ni/Al	900-900-9-1	0.042
Ni/Al	900-900-9-2	0.040
Ni-Mg/Al	900-900-9-1	0.046
Ni/Al	900-900-9-2	0.039

lysts is less than 0.04 g/g, which is minor except for 750-900-9-2 which has the value of 0.197 g/g. It is indicated that the influence of T_1 is the most significant by comparing the different reaction temperatures and S/C values. When T_1 is higher, the initial hydrocracking of MNP is sufficient; therefore, no obvious carbon deposition is found for the used catalysts in TSR. However, when T_1 is lower but T_2 is higher, the evident carbon deposition tends to be generated in the catalyst of SR, which can be attributed to the limited hydrocracking of MNP in FR and enhanced thermal decomposition in SR. However, few differences of the carbon depositions are found when S/B is increased from 9 to 12 as shown in Fig. 15(b); hence, there is no need for introducing excess steam to reduce carbon deposition.

From Fig. 15(c) and Table 6, a few carbon depositions on the catalysts of Ni/Al and Ni-Mg/Al can also be found, which are a little more than those of Ni-Li/Al. As for Ni-Mg/Al, especially, the carbon deposition is 0.046 g/g and the weight decreases by 3% after 600 °C, revealing that it can only be converted at higher temperatures [37]. It is indicated that the modification of Mg tends to influence the components of carbon deposition, resulting in a small amount of comparatively stable carbon deposited in the Ni-Mg/Al of FR.

7-2. XPS Analysis

As for the catalyst samples of Ni-Li/Al used at 750-900-9-2 and Ni-Mg/Al used at 900-900-9-1, the C1s binding energies were analyzed by XPS to study the species and fractions of carbon deposition. The obtained spectra and fractions are presented in Fig. 16 and Table 7, respectively.

The C1s spectra of two catalyst samples are each resolved into different component peaks. The peak at 284.6 eV corresponds to C-C, while the peaks located at 286.1 eV and 288.1 eV are assigned to C-O and C=O, respectively [37,38]. For Ni-Mg/Al, the peak at 283.9 eV is corresponding to Ni carbide-like species (Ni_xC) [39].

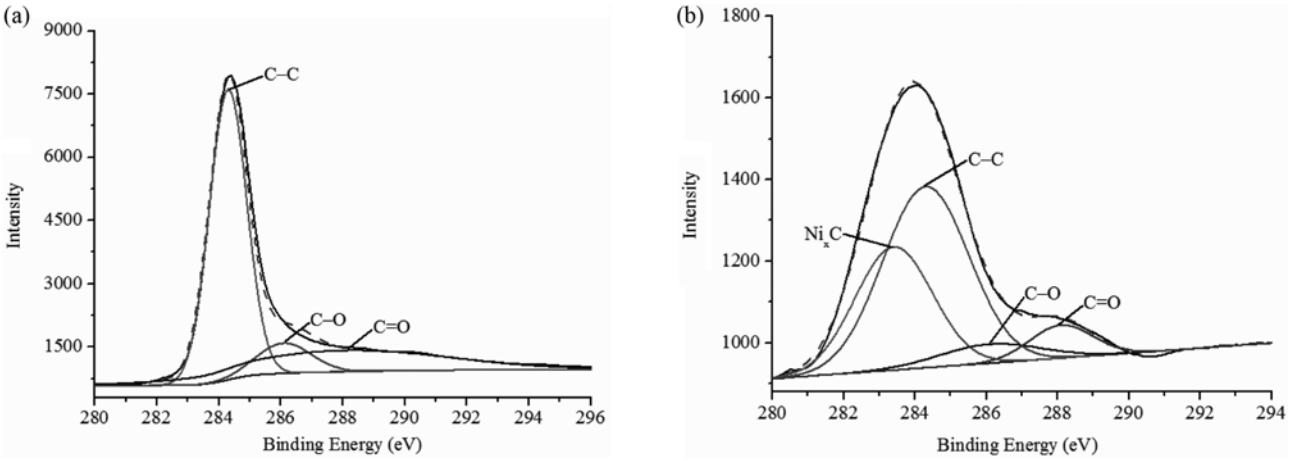

Fig. 16. C1s spectra of catalysts. (a) Ni-Li/Al used at 750-900-9-2, (b) Ni-Mg/Al used at 900-900-9-1.

Table 7. Assignment and fractions of carbon species from C1s spectra

Samples	Molar concentrations (%)			
	Ni_xC	C-C	C-O	C=O
Ni-Li/Al used at 750-900-9-2	0.0	64.3	9.6	26.1
Ni-Mg/Al used at 900-900-9-1	32.7	53.6	6.6	7.1

With respect to the 750-900-9-2, C-C takes up the major proportion while less C=O and C-O are also contained in this sample without Ni_xC. Furthermore, the deposited carbon can be converted efficiently at 500 °C, indicating that the major carbon species are amorphous carbon [36] and oxycarbides containing C=O. As for Ni-Mg/Al, C-C and Ni_xC account for the majority of carbon species with slight C-O and C=O included. In addition, the deposited carbon can only be removed above 600 °C, revealing that the dominant components of carbon deposition can be Ni carbide-like species and well developed carbon fibers or graphite with lower reactivity.

CONCLUSIONS

An experimental study on the steam reforming of MNP employing Ni-Li/Al was conducted for hydrogen-rich gas in the two-stage reactor (TSR), and the catalytic effects of Ni-Li/Al were also compared with that of Ni/Al and Ni-Mg/Al. The conclusions are as follows:

(1) The influence of FR temperature (T_1) on the X_C and R_{H2} of MNP reforming is most significant, while the significances of SR temperature (T_2) and S/C are close in the response surface experiments using Ni-Li/Al in TSR. The optimization results show that when T_1 and T_2 are both 900 °C and S/C reaches 9, X_C and R_{H2} could rise to 76.1% and 120.2 mol/kg-tar to the maximum, matching well with the experimental results.

(2) Appropriate hydrogenation is able to remarkably improve the overall reforming effect of MNP, especially at lower temperatures. When T_1 and T_2 are 750 °C, the conversion effects of X_C and R_{H2} can still be superior to that of the optimization results at 900 °C without hydrogenation. Hydrogenation could be realized by partially cycling the product gas into the reforming reactor during biomass steam gasification for H_2-rich gas to improve tar conversion.

(3) Ni-Li/Al and Ni-Mg/Al exhibit similar effect on the initial hydrocracking of MNP, while the catalytic activity of Ni/Al is mainly embodied in the promotion to reforming and water gas shift reactions. It is more efficient in the conversion to load Ni-Li/Al or Ni-Mg/Al in FR while using Ni/Al in SR.

(4) When T_1 is high enough, the initial hydrocracking is relatively sufficient, and there is no obvious carbon deposition in the catalysts. Additionally, the carbon deposition resistance of Ni-Li/Al is better than that of Ni-Mg/Al and Ni/Al.

ACKNOWLEDGEMENT

This work was supported by the National Natural Science Foundation of China (51576047, 51576048).

NOMENCLATURE

X_C : carbon conversion efficiency [%]
R_{H2} : hydrogen yield [mol/-tar]
n_i : mole number of gas i (CO, CO_2 and CH_4) [mol/kg-tar]
C_{ni} : concentration of gas i (CO, CO_2 and CH_4) [-]
MW_C : molar mass of carbon [g/mol]
W_C : carbon content per kg MNP [g/kg]
V_{H2} : volume of produced hydrogen under normal temperature and pressure [L]
m : mass of MNP introduced [kg]
T_1 : temperatures of the first reactor [°C]
T_2 : temperatures of the second reactor [°C]
S/C : molar ratios of steam to carbon [-]

REFERENCES

1. G. Q. Guan, M. Kaewpanha, X. G. Hao and A. Abudula, *Renew Sust. Energy Rev.*, **58**, 450 (2016).
2. F. M. Josuinkas, C. P. B. Quitete, N. F. P. Ribeiro and M. M. V. M.

Souza, *Fuel Proc. Technol.*, **121**, 76 (2014).
3. H. Balat and E. Kırtay, *Int. J. Hydrogen Energy*, **35**, 7416 (2010).
4. N. Nipattummakul, I. I. Ahmed, S. Kerdsuwan and A. K. Gupta, *Int. J. Hydrogen Energy*, **35**, 11738 (2010).
5. C. Franco, F. Pinto, I. Gulyurtlu and I. Cabrita, *Fuel*, **82**, 835 (2003).
6. L. Devi, K. J. Ptasinski and F. J. Janssen, *Biomass Bioenergy*, **24**, 125 (2003).
7. D. Swierczynski, C. Courson and A. Kiennemann, *Chem. Eng. Process.*, **47**, 508 (2008).
8. K. Polychronopoulou, K. Giannakopoulos and A. M. Efstathiou, *Appl. Catal. B: Environ.*, **111**, 360 (2012).
9. J. I. Ozaki,; M. Takei,; K. Takakusagi and N. Takahashi, *Fuel Proc. Technol.*, **102**, 30 (2012).
10. Y. L. Zhang, Y. H. Luo, W. G. Wu, S. H. Zhao and Y. F. Long, *Energy Fuels*, **28**, 3129 (2014).
11. J. Ashok and S. Kawi, *Acs Catal.*, **4**, 289 (2014).
12. T. J. Wang, J. Chang, C. Z. Wu, Y. Fu and Y. Chen, *Biomass Bioenergy*, **28**, 508 (2005).
13. T. Furusawa and A. Tsutsumi, *Appl. Catal. A: Gen.*, **278**, 195 (2005).
14. L. Devi, K. J. Ptasinski and F. J. J. G. Janssen, *Fuel Proc. Technol.*, **86**, 707 (2005).
15. R. Michel, A. Łamacz, A. Krzton, G. Djega-Mariadassou, P. Burg, C. Courson and R. Gruber, *Fuel*, **109**, 653 (2013).
16. R. Zhang, Y. Wang and R. C. Brown, *Energy Convers. Manage.*, **48**, 68 (2007).
17. D. Li, Y. Nakagawa and K. Tomishige, *Chinese J. Catal.*, **33**, 583 (2012).
18. T. Miyazawa, T. Kimura, J. Nishikawa, S. Kado, K. Kunimori and K. Tomishige, *Catal. Today*, **115**, 254 (2006).
19. M. L. Dieuzeide, M. Laborde, N. Amadeo, C. Cannilla, G. Bonura and F. Frusteri, *Int. J. Hydrogen Energy*, **41**, 157 (2016).
20. J. Yang, X. G. Wang, L. Li, K. Shen, X. G. Lu and W. Z. Ding, *Appl. Catal. B: Environ.*, **96**, 232 (2010).
21. C. X. Qi, J. C. Amphlett and B. A. Peppley, *J. Power Sources*, **171**, 842 (2007).
22. P. Kuchonthara, B. Puttasawat, P. Piumsomboon, L. Mekasut and T. Vitidsant, *Korean J. Chem. Eng.*, **29**(11), 1525 (2012).
23. T. Osaki and T. Mori, *J. Catal.*, **204**, 89 (2001).
24. L. H. Kong, B. H. Yue, X. G Wang, F. Yu, Q. Zhen, X. Q. Lu and W. Z. Ding, *Chinese J. Process. Eng.*, **9**(2), 403 (2009).
25. X. H. Nguyen, W. Bae, T. Gunadi and Y. Park, *J. Petrol. Sci. Eng.*, **117**, 37 (2014).
26. J. Fermoso, M. V. Gil, B. Arias, M. G. Plaza, C. Pevida, J. J. Pis and F. Rubiera, *Int. J. Hydrogen Energy*, **35**, 1191 (2010).
27. N. M. Deraz, H. H. Salim and A. A. El-Aal, *Mate. Lett.*, **53**, 102 (2002).
28. G. H. Li, L. J. Hu and J. M. Hill, *Appl. Catal. A: Gen.*, **301**, 16 (2006).
29. J. Juan-Juan, M. C. Roman-Martinez and M. J. Illan-Gomez, *Appl. Catal. A: Gen.*, **301**, 9 (2006).
30. O. Dewaele and G. F. Froment, *J. Catal.*, **184**, 499 (1999).
31. J. L. Pinilla, P. Arcelus-Arrillaga, H. Puron and M. Millan, *Fuel*, **109**, 303 (2013).
32. X. Lv, J. Xiao, Y. Z. Du, L. H. Shen and Y. Y. Zhou, *Int. J. Hydrogen Energy*, **39**, 20968 (2014).
33. P. Parthasarathy and K. S. Narayanan, *Renew. Energy*, **66**, 570 (2014).
34. Y. Shen and K. Yoshikawa, *Renew. Sust. Energy Rev.*, **21**, 371 (2013).
35. G. Oh, S. Y. Park, M. W. Seo, Y. K. Kim, H. W. Ra, J. Lee and S. J. Yoon, *Renew. Energy*, **86**, 841 (2016).
36. L. Chen, Z. D. Hao, T. Z. Yang, W. F. Liu and D. C. Zhang, *Int. J. Hydrogen Energy*, **39**, 15474 (2014).
37. L. Guczi, G. Stefler, O. Geszti, I. Sajo, Z. Paszti, A. Tompos and Z. Schay, *Appl. Catal. A: Gen.*, **375**, 236 (2010).
38. X. E. Verykios, *Int. J. Hydrogen Energy*, **28**, 1045 (2003).
39. C. Z. Wang, N. N. Sun, N. Zhao, W. Wei, Y. H. Sun, C. G. Sun, H. Liu and C. E. Snape, *Fuel*, **143**, 527 (2015).